PCCP

PAPER

View Article Online
View Journal | View Issue

Published on 09 September 2014. Downloaded by Tokyo Metropolitan University on 23/10/2014 09:00:16.

Cite this: *Phys. Chem. Chem. Phys.*, 2014, **16**, 23663

Remarkable enhancement of the photoreactivity of a polyfluoroalkyl azobenzene derivative in an organic–inorganic nano-layered microenvironment†

Vivek Ramakrishnan,[a] Daisuke Yamamoto,[ab] Shin Sasamoto,[a] Tetsuya Shimada,[ab] Yu Nabetani,[ab] Hiroshi Tachibana[ab] and Haruo Inoue*[ab]

Received 8th August 2014,
Accepted 8th September 2014

DOI: 10.1039/c4cp03549f

www.rsc.org/pccp

Organic–inorganic hybrids composed of polyfluoroalkyl azobenzene surfactant (abbreviated as C3F-Azo-C6H) and inorganic layered compounds are able to undergo reversible three-dimensional morphology changes such as interlayer space changes and nanosheet sliding in a giant scale due to reversible *trans–cis* isomerization of the azobenzene moiety upon photo-irradiation. In this paper, we have systematically studied the relationship between the layered hybrid microstructures of C3F-Azo-C6H–clay and their photoreactivity for understanding the mechanism of the photo-induced morphology change. The photoreactivity was found to be very much affected by the surrounding microenvironments. As compared with it in solution, the *cis–trans* photo-isomerization in C3F-Azo-C6H–clay nano-layered film was substantially enhanced with the quantum yield exceeding unity (Φ = 1.9), while the *trans–cis* isomerization was rather retarded. The corresponding hydrocarbon analogue of the azobenzene surfactant (C3H-Azo-C6H) did not show such an enhancement. The enhancement was discussed in terms of a cooperative effect among adjacent azobenzene moieties along with polyfluoroalkyl chains and the inorganic clay nanosheet to prevent a dissipation of the excess energy being liberated during the photo-isomerization within the nano-layered microenvironment.

Introduction

Various kinds of supra-molecular system have been developed and their reactivity and functionality have been well studied in the past few decades.[1] Research interest is currently advancing into supra-molecular systems coupled with the surrounding microenvironments.[2,3] Many kinds of material such as micelle, vesicle, liquid crystal, layered compounds, mesoporous materials, biomaterials such as proteins and so on have been expected to be prospective candidates as microenvironments for developing sophisticated functions. Layered compounds are also among the most promising materials as microenvironments, which can provide unique two-dimensional interlayer spaces to the supra-molecular systems. So far, many kinds of layered compound have been studied in terms of their synthesis,[4–6] exfoliation,[7–12] intercalation,[13,14] electrochemical properties,[15] optical properties,[16] catalysis,[17] photocatalysis[18–20] and so on. In particular, the intercalation of organic molecules into the interlayer spaces can provide various interesting functions such as fluorescence enhancement,[21,22] efficient energy transfer[23] and electron transfer,[24] catalytic reactions,[14,25,26] dye-sensitized solar cells (DSSC)[27] and artificial photosynthesis[28] and so on.

Molecular assemblies of polyfluorinated surfactants and their hybrids with layered compounds and mesoporous materials have been successfully fabricated and studied as novel micro-environments for photochemical reactions in our group. The surface polyfluorinated micelles and vesicles can provide unique microenvironments for photochemical reactions owing to their high resistance to oxidation and the high solubility of gases as compared with hydrocarbons.[29,30]

Hybrids with layered compounds such as clay minerals (Sumecton SA: SSA), whose crystal structure is shown in Fig. 1a, can be successfully fabricated by the intercalation of polyfluorinated surfactant molecules (CnF-S).[31–33] These polyfluorinated molecules were found to intercalate in amounts exceeding the cation exchange capacity (CEC). In particular, C3F-S exhibited intercalation up to 4.4 eq. *versus* CEC as a saturated adsorption limit.[31] For providing some photo-responsive moiety to the

[a] *Department of Applied Chemistry, Tokyo Metropolitan University, 1-1 Minami-osawa, Hachioji, 192-0397, Japan. E-mail: inoue-haruo@tmu.ac.jp*
[b] *Center for artificial photosynthesis, Tokyo Metropolitan University, 1-1 Minami-osawa, Hachioji, 192-0397, Japan*

† Electronic supplementary information (ESI) available: Fig. S1. XRD chart for C3F-Azo-C6H/Clay swelled with solvents. Fig. S2. (a–g) Quantum yield measurement data. Fig. S3. (a–q) Activation energy determination. See DOI: 10.1039/c4cp03549f

Published on 09 September 2014. Downloaded by Tokyo Metropolitan University on 23/10/2014 09:00:16.

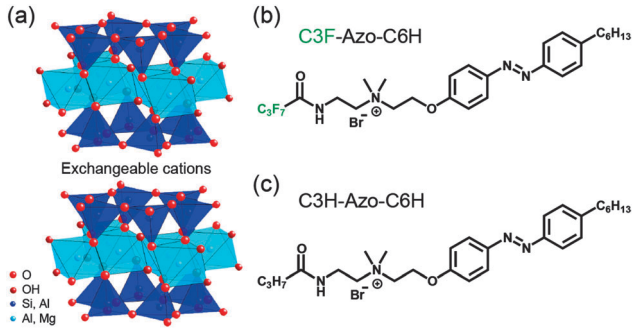

Fig. 1 Crystal structure of (a) an inorganic layered clay mineral, Sumecton SA, and chemical structures of (b) polyfluorinated cationic surfactant (C3F-Azo-C6H) and (c) alkylated cationic surfactant (C3H-azo-C6H).

hybrids, we have also fabricated hybrids composed of polyfluoroalkyl azobenzene surfactant (C3F-Azo-C6H) and potassium hexaniobate ($K_4Nb_6O_{17}$). Such kinds of photo-responsive layered hybrid show a high-density adsorption of C3F-Azo-C6H on the niobate nanosheets similar to that of the SSA hybrids because of the small intermolecular interaction of the polyfluoroalkyl chain.

Most interestingly, we have found that three-dimensional morphology changes can be induced on the hybrids by a *trans–cis* photo-isomerization reaction of the azobenzene group within the polyfluorinated cationic surfactants.[2,3,34] One of the highlights is a horizontal sliding of the nanosheets in a giant scale of ~1500 nm.[3] How can such a giant scale change be induced by a molecular shape change on the nm scale? The system may be taken as one of artificial muscle model units. It should thus be most interesting to clarify the molecular mechanism of the horizontal sliding of the nanosheets. Though the detailed mechanism is not fully revealed, it is convincing that the photo-isomerization reaction of C3F-Azo-C6H in the interlayer space sandwiched by nanosheets as a microenvironment is actually inducing morphology changes such as interlayer distance change and nanosheet sliding. To get a deeper insight into the morphological change in nano-layered organic–inorganic hybrid compounds, we firstly studied systematically how the photo-isomerization of the azobenzene moiety within the polyfluorinated surfactant is affected by various microenvironments.

The photo-isomerization reaction of azobenzene and its derivatives have been studied by UV-vis spectroscopy,[35] time-resolved transient absorption spectroscopy[36,37] and time-resolved Raman spectroscopy[37,38] in the past few decades.

In this paper, we have investigated systematically the reactivity of a molecular assembly of polyfluoroalkyl azobenzene derivative confined within the inorganic nanosheets of clay mineral in terms of its quantum yield. The molecular assemblies of C3F-Azo-C6H in the interlayer spaces of the clay hybrid showed remarkable enhancement of reactivity for the *cis* to *trans* isomerization reaction upon visible light irradiation. The enhancement was discussed in terms of the cooperative effect among adjacent azobenzene moieties along with polyfluoroalkyl chains and the inorganic clay nanosheet to prevent a dissipation of the excess energy being liberated during the photo-isomerization within the nano-layered microenvironment.

Results and discussion

Intercalation of C3F-Azo-C6H into the interlayer spaces of SSA

Nanosheets of synthetic inorganic clay, SSA, can be easily exfoliated in water and form a hybrid by intercalation of cationic molecules such as surfactants.[31,39] Fig. 2a shows an adsorbed amount of polyfluoroalkyl cationic surfactant having an azobenzene moiety, C3F-Azo-C6H, *versus* CEC of SSA being dependent upon the loading level. With an increase in the loading level, the adsorbed amount increased and became saturated over the loading level of 15 eq. *versus* CEC. In the saturated region, the adsorbed amount was 4.2 eq. *versus* CEC, which is in good agreement with that of C3F-S–SSA reported previously.[30] In the case of loading level 20 eq. *versus* CEC, the occupied area per one molecule adsorbed on the surface of SSA estimated by thermogravimetric analysis (TGA) was 28 Å^2, which is very similar to the cross-sectional area of the polyfluoroalkyl chain. The occupied area (28 Å^2) clearly indicates that the polyfluorinated cationic surfactant formed a bilayer structure within the interlayer space, since an occupied area for a monolayer structure should give an area of twice the cross-sectional one. It is considered that C3F-Azo-C6H could be densely adsorbed on the surface of the SSA nanosheet due to the strong hydrophobicity and lipophobicity of the polyfluoroalkyl chain. The XRD patterns of the C3F-Azo-C6H–SSA hybrids at each loading level are shown in Fig. 2b. With increasing loading level, the d_{001} peak gradually shifted to a smaller angle.

Fig. 3 shows how the basal spacing d_{001} of the original SSA[31] changed against the adsorbed amount of C3F-Azo-C6H *versus* CEC in the hybrids. With an increment of the adsorbed amount of C3F-Azo-C6H, the interlayer distance expanded and reached a saturated distance, 3.4 ± 0.1 nm, at around 2.3 eq. *versus* CEC. The interlayer distance of the hybrid was kept constant for the further intercalation, while the adsorbed amount of C3F-Azo-C6H increased as shown in Fig. 2a. As observed in the previous C3F-S intercalation to SSA,[31] the C3F-Azo-C6H molecule can also induce the formation of a well-aligned structure.

The interlayer distance (3.4 ± 0.1 nm) at the saturated condition and the molecular length of C3F-Azo-C6H (3.2 nm) suggest that the C3F-Azo-C6H adsorbed with a tilting angle of 58° to the normal line of the nanosheet surface of SSA. Since

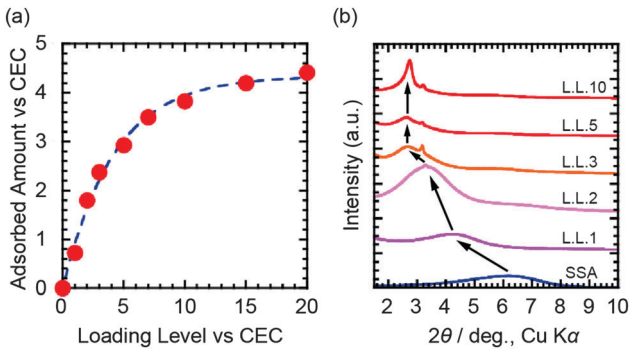

Fig. 2 (a) Adsorbed amounts of C3F-Azo-C6H (*versus* CEC) against the loading levels (L. L.) and (b) X-ray diffraction patterns of the C3F-Azo-C6H–SSA hybrid films at each loading level.

This journal is © the Owner Societies 2014

Published on 09 September 2014. Downloaded by Tokyo Metropolitan University on 23/10/2014 09:00:16.

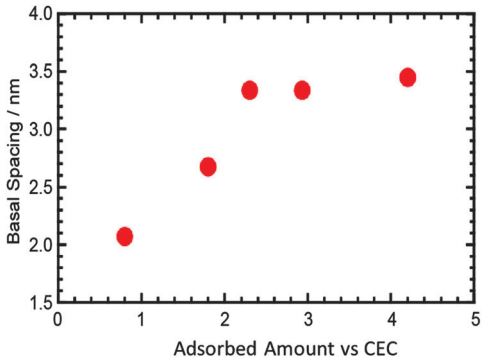

Fig. 3 The basal spacing d_{001} of the hybrids against the adsorbed amount of C3F-Azo-C6H *versus* CEC.

C3F-Azo-C6H forms a bilayer, the tilting angle θ is calculated by $\cos\theta = (3.4/2)/3.2$.

The interlayer spaces of such layered hybrids may be able to incorporate other molecules such as solvent. To check this possibility, XRD signals on the hybrid film swelled with benzene or *n*-hexane were compared with the hybrid film under the dry condition. The XRD patterns of the hybrid swelled with organic solvents are shown in Fig. S1 (ESI†). The hybrid film swelled with benzene showed the diffraction peak shift to the lower angle as compared with that dried in vacuum (Fig. S1a, ESI†). This indicates that the interlayer distance of the hybrid expanded from 3.45 nm to 3.62 nm by the intercalation of benzene molecules. Furthermore, the XRD peak came back to the original position (3.39 nm) by drying in vacuum again. On the other hand, no diffraction peak shift was observed in the hybrid swelled with *n*-hexane (Fig. S1b, ESI†), indicating that *n*-hexane molecules could not penetrate into the interlayer spaces of the hybrid.

Photoreaction of C3F-Azo-C6H–SSA hybrids

The spectral characteristics of C3F-Azo-C6H observed in the photo-isomerization of the azobenzene moiety (Fig. 4) in various microenvironments are summarized in Table 1. The absorption peak assigned to the π–π* transition of the *trans*-form of C3F-Azo-C6H is at around 344 nm, which is known to exhibit a red-shift by a J-type intermolecular interaction and a blue-shift through an H-type intermolecular interaction according to Kasha's exciton

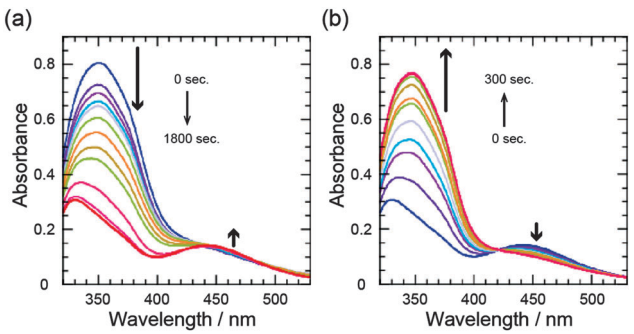

Fig. 4 Absorption spectral changes of C3F-Azo-C6H–SSA film (4.2 eq. *vs.* CEC) in air upon (a) UV and (b) visible light irradiation.

Table 1 Spectral characteristics of C3F-Azo-C6H in various microenvironments

Sample	λ_{trans}/nm	λ_{cis}/nm	$\lambda_{Isosbestic}$/nm
C3F-Azo-C6H in ethanol	344	440	403
C3F-Azo-C6H in water	346	434	421
Hybrid film in air	347	442	420
Hybrid film in benzene	347	441	410
Hybrid film in *n*-hexane	345	443	413

model.[40] It should be a good measure to observe the shift of the λ_{max} for getting information on how the azobenzene moieties are mutually interacting in each microenvironment. The λ_{max} of C3F-Azo-C6H in ethanol, where C3F-Azo-C6H is believed to be solubilized as a monomer molecule without mutual interaction, may be taken as the standard in judging it. All the λ_{max} values under other conditions, such as in water where a micelle is formed at the concentration 3.3×10^{-5} M examined here, in the hybrid film under the dry condition, and in the hybrid film swelled with benzene and with *n*-hexane, exhibited a slight red-shift, indicating a mutual J-type interaction between the adjacent molecules in each microenvironment. Though it is somewhat difficult to estimate the precise spectral peak due to the light scattering of the film sample, similarly, the isosbestic points of their spectra, where the scattering contribution is fairly small, also showed a clear red shift. Since C3F-Azo-C6H is tilting against the surface of the clay nanosheet, the red-shifts may be thus rationalized. On the other hand, the λ_{max} of the *cis*-form (n–π* transition) showed a substantial blue-shift only in water. This strongly suggests that even in micelle, water molecules penetrate into the inner core, azobenzene moieties, to form intermolecular hydrogen bonds.

Fig. 4 shows the absorption spectra of the C3F-Azo-C6H–SSA hybrid film in air upon photo-irradiation. The hybrid film had fairly good transparency probably due to the well ordered bilayer structure caused by the introduction of polyfluoroalkyl chain, and the absorption spectra were measured by an ordinary spectroscopic method. Upon UV light (λ = 365 nm) irradiation, the peak at 347 nm decreased drastically. In contrast, the absorption at around 442 nm, which is assigned to the n–π* transition of the *cis*-form of azobenzene, slightly increased and finally reached a photo-stationary state (PSS).

On the other hand, the photo-isomerization reaction from the *cis*- to the *trans*-form was efficiently induced by visible light irradiation. The hybrid film, once irradiated with UV light to become rich in the *cis*-form of azobenzene, showed very efficient reversion to the *trans*-form upon visible light irradiation (λ = 453 nm). To get a deeper insight into what is happening within the interlayer spaces composed of polyfluoroalkyl cationic surfactant molecules and the inorganic nanosheets, a systematic observation of the photo-isomerization of the surfactant with azobenzene group in various microenvironments was carried out. The transparency of the hybrid film was sufficient to enable an estimate of the photo-reactivity in terms of quantum yield. The quantum yield for the photo-isomerization reaction of C3F-Azo-C6H in each microenvironment was estimated by the absorption spectral changes. The number of molecules converted in the reaction

Published on 09 September 2014. Downloaded by Tokyo Metropolitan University on 23/10/2014 09:00:16.

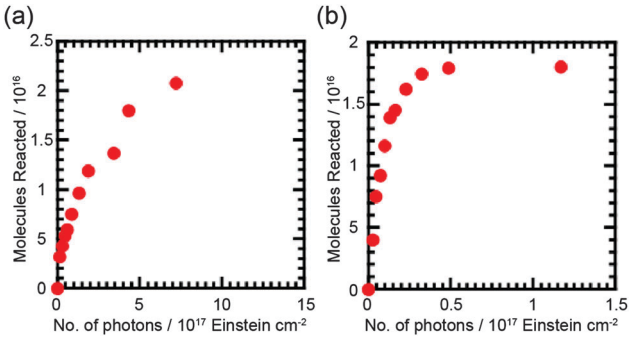

Fig. 5 Molecules converted for C3F-Azo-C6H–SSA film (4.2 eq. *vs.* CEC) estimated from the absorption at 365 nm upon (a) UV and (b) visible light irradiation.

was calculated from the change of absorption for the π–π* transition because the absorption change at around 450 nm was somewhat smaller as compared with that at around 350 nm. Fig. 5 shows the number of molecules converted for C3F-Azo-C6H–SSA film estimated from the absorption at 365 nm upon UV and visible light irradiation. At the initial stage of the photoreaction, the conversion increased drastically with a gradual decrease of the slope and finally the reaction reached the PSS. The initial slope of the time course of the reaction should correspond to the quantum yield for the photo-isomerization reaction. The internal filtering effect by the product molecules (*trans*-form) themselves should be taken into account for the *cis–trans* isomerization reaction as described in the Experimental section. Furthermore, the light scattering effect in the case of film samples for estimating the number of photons actually absorbed by the azobenzene moiety should also be considered for the calculation of the quantum yield (see the Experimental section). On the basis of such careful treatment of the data, the quantum yields of the photo-isomerization for C3F-Azo-C6H in various microenvironments are summarized in Table 2 (see also Fig. S2a–g, ESI†).

The *trans* to *cis* isomerization reaction of C3F-Azo-C6H–SSA film was rather retarded ($\Phi_{trans-cis}$ = 0.13) compared with those in ethanol ($\Phi_{trans-cis}$ = 0.35) and micelle (water ($\Phi_{trans-cis}$ = 0.42)). Very interestingly, however, the *cis–trans* isomerization reaction of C3F-Azo-C6H–SSA in the hybrid film was remarkably enhanced compared with that in ethanol ($\Phi_{cis-trans}$ = 0.64) and the quantum yield exceeded unity! The quantum yield of C3F-Azo-C6H was estimated to be $\Phi_{cis-trans}$ = 1.9 in the microenvironment of hybrid film under air atmosphere. Furthermore, a similar enhancement

Table 2 The quantum yields of the photo-isomerization reaction in various microenvironments

Sample/microenvironment	$\Phi_{trans-cis}$	$\Phi_{cis-trans}$
C3F-Azo-C6H/ethanol	0.35	0.64
C3F-Azo-C6H/micelle	0.42	0.79
C3F-Azo-C6H–SSA film/benzene	0.18	0.94
C3F-Azo-C6H–SSA film/*n*-hexane	0.10	1.1
C3F-Azo-C6H–SSA film/air	0.13	1.9
C3H-Azo-C6H/ethanol	0.35	0.63
C3H-Azo-C6H/micelle	0.36	0.77
C3H-Azo-C6H–SSA film/air	0.09	0.42

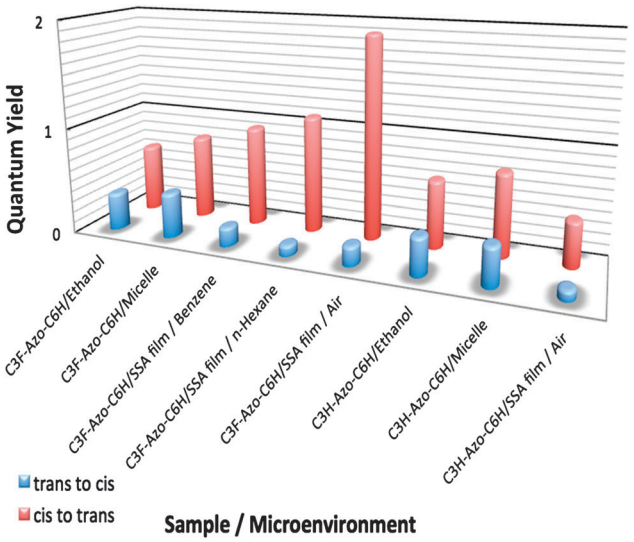

Fig. 6 The quantum yield of cationic azobenzene surfactants and their hybrids with SSA.

was observed in the C3F-Azo-C6H–SSA hybrid film moistened with benzene ($\Phi_{cis-trans}$ = 0.94) and *n*-hexane ($\Phi_{cis-trans}$ = 1.1). The hybrid moistened with *n*-hexane showed higher reactivity than that with benzene.

On the other hand, both the *trans–cis* ($\Phi_{trans-cis}$ = 0.09) and the *cis–trans* ($\Phi_{cis-trans}$ = 0.42) isomerization reactions of the C3H-Azo-C6H–SSA film in the air were not so efficient when compared with those of C3F-Azo-C6H. The quantum yields of azobenzene derivatives in various microenvironments are shown three-dimensionally in Fig. 6. The efficiency of the *trans–cis* isomerization reaction of C3F-Azo-C6H systematically decreased with an increase of the rigidity in the microenvironment (EtOH < micelle < hybrid film swelled with solvent < hybrid film under dry conditions), while the reactivity was in the opposite order for *cis–trans* isomerization. The corresponding hydrocarbon analogue, C3H-Azo-C6H–SSA, was rather independent of the tendency. To understand the reactivity of the photo-isomerization reaction, especially with regard to the enhanced reactivity for the *cis–trans* isomerization in each microenvironment, it may be necessary to consider the possibility of a contribution by a thermal process of azobenzene.

Thermal isomerization of azobenzene in the dark

The thermally induced *cis–trans* isomerization reaction of azobenzene is well known and has been studied by many researchers.[35] Fig. 7a shows the time course of the absorption spectral change of C3F-Azo-C6H–SSA film at 28 °C in the dark. The absorption at 442 nm identified as a *cis*-form of C3F-Azo-C6H decreased and finally the absorption spectrum of *trans*-C3F-Azo-C6H–SSA film was obtained after 1400 sec. The rate of the reaction is analyzed in Fig. 7b. The *cis–trans* isomerization of C3F-Azo-C6H–SSA film was very slow and the pseudo-first order rate constant, *k*, for the thermal isomerization was estimated to be 2.0×10^{-5} s^{-1} in the dark. It is thus concluded that the contribution of a thermal process provided from the experimental environment (surrounding heat-bath) is negligibly small compared with the photochemical one, because

 This journal is © the Owner Societies 2014

Published on 09 September 2014. Downloaded by Tokyo Metropolitan University on 23/10/2014 09:00:16.

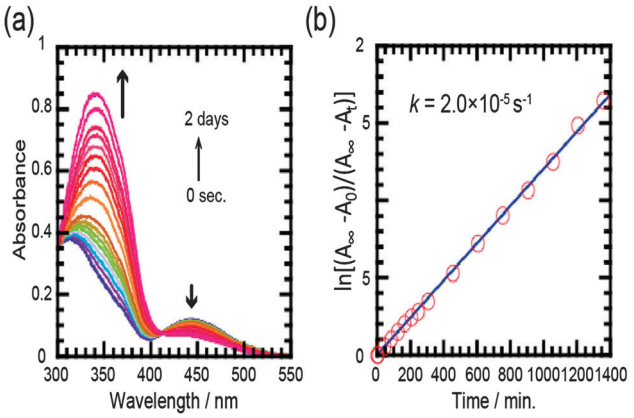

Fig. 7 Thermal reactivity of C3F-AzoC6H–SSA film: (a) the absorption spectral change; and (b) the rate of the *cis* to *trans* isomerization reaction of C3F-Azo-C6H–SSA film (4.2 eq. *vs.* CEC) preserved at 28 °C.

the quantum yields of all photoreactions of C3F-Azo-C6H or C3H-Azo-C6H were measured within the initial several tens of seconds when the rate constant (2.0×10^{-5} s^{-1}) indicates the contribution of the thermal process is negligible.

Though the thermal process induced by the surrounding heat-bath was revealed to be negligible, the C3F-Azo-C6H molecule obtains energy of 0.545 aJ and 0.452 aJ per one photon by 365 nm and 440 nm excitations, respectively. How could the absorbed energy be utilized?

Energy state diagram of azobenzene

Before discussing how the absorbed energy would be utilized for the isomerization reaction, it is crucial to understand the energy state diagram of azobenzene derivatives. According to the previous reports on azobenzene,[41,42] the energy state S_0 (*trans*- and *cis*-form), S_1 (*trans*- and *cis*-form), and S_2 (*trans*- and *cis*-form) states are depicted as in Fig. 8a. The *cis*-form is destabilized by ~50 kJ mol^{-1} than the *trans*-form and the transition state (TS) in the ground state lies above the *cis*-form (S_0) by ~92 kJ mol^{-1}, while the potential energy surfaces in the excited states are not so straightforward. The activation energy for the thermal conversion of *cis*- into *trans*-form was reported to be ~92 kJ mol^{-1} for azobenzene and here we also studied the activation energy for the conversion of *cis*- into *trans*-form for C3F-Azo-C6H in various microenvironments. (Fig. S2a–q, ESI†). As summarized in Table 3, the activation energy for C3F-Azo-C6H in ethanol (111 kJ mol^{-1}) was a little larger with azobenzene itself (92 kJ mol^{-1}), while in other microenvironments such as micelle (99 kJ mol^{-1}), C3F-Azo-C6H–clay dispersed in benzene (102 kJ mol^{-1}), and C3F-Azo-C6H–clay film (98 kJ mol^{-1}) the activation energy for the conversion from *cis*- into *trans*-form decreased in every case as compared with that in ethanol. These results strongly suggest that the *cis*-form with increased free volume is more destabilized in more rigidly packed microenvironments such as micelle and hybrid interlayers. Level-crossing between the two parabolas of the ground state potential energy of the *trans*-form and the *cis*-form as depicted in Fig. 8b could explain how the activation energy would change upon the

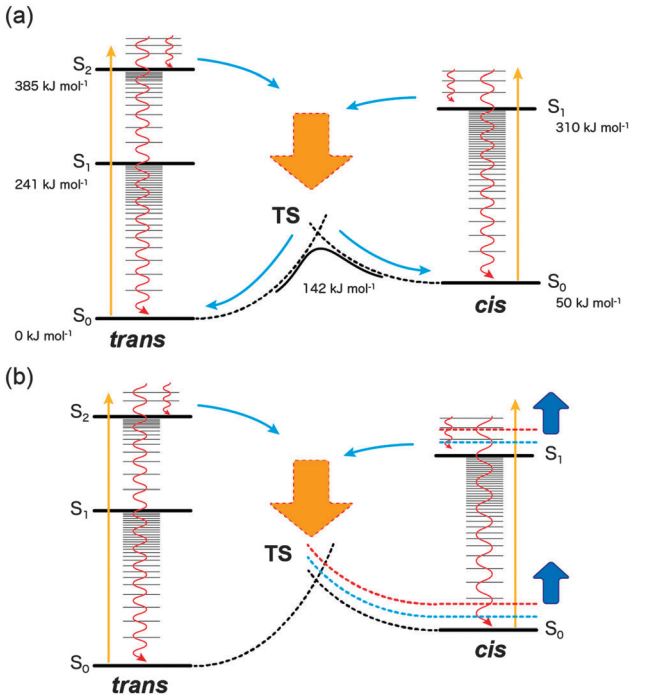

Fig. 8 Schematic illustration of energy state diagrams for photo-isomerization: (a) unsubstituted azobenzene and (b) C3F-Azo-C6H in microenvironment.

Table 3 The activation energy of *cis*–*trans* isomerization of C3F-Azo-C6H in various microenvironments

Sample/microenvironment	Activation energy/kJ mol^{-1}
C3F-Azo-C6H/ethanol	111
C3F-Azo-C6H/micelle	99
C3F-Azo-C6H–SSA film/benzene	102
C3F-Azo-C6H–SSA film/air	98

further destabilization of the *cis*-form with increased free volume in the more rigid microenvironment. The actually observed decrease of the activation energy suggests the further destabilization of the *cis*-form and also suggest that the structure of the TS becomes closer to the *cis*-form, since the crossing point moves towards the *cis*-form. The situation would lead to a presumption that upon excitation of molecules to the excited state either of S_1 (*trans* or *cis*) or S_2 (*trans* or *cis*), relaxation down to the ground state potential energy surface may preferably afford the *trans*-form, depending on level-crossing of potential energy surfaces within the excited states and with those of the ground states. The presumption well explains the systematic enhancement of *cis*–*trans* isomerization in micelle and hybrid nano-layers. The remarkable enhancement of the quantum yield exceeding unity, however, still needs further explanation. Even when the enhancement is induced by the further destabilization of the *cis*-form in rigid microenvironment, the maximum limit of the quantum yield should be smaller than unity! Some other factor such as a cooperating effect among the adjacent molecules should be operative in the hybrid nano-layered microenvironment

Published on 09 September 2014. Downloaded by Tokyo Metropolitan University on 23/10/2014 09:00:16.

in addition to the above mentioned effect on the potential energy surfaces. Further consideration can be made as follows on this point.

After the photo-excitation, the excited molecule in the Franck–Condon state either in S_2 (π–π^*) or S_1 (n–π^*) would relax to the lowest vibrational level of the excited states with liberation of excess vibrational energy and the reaction into the *cis*- or *trans*-form proceeds also with liberation of excess energy. In general, most of the excess energy liberated upon vibrational relaxation or on the reaction pathway is immediately dissipated through intramolecular vibrational modes and equilibrated among them within the corresponding molecule. And subsequently the equilibrated excess energy is further dissipated to the surrounding media such as solvent molecules through V–V and V–T processes.[43,44] In fluid solution such as ethanol, all the dissipation processes should be completed within *ca.* ten picoseconds time scale and the photochemically excited molecule is rapidly quenched to be thermally equilibrated with the surrounding solvent molecules as the external heat-bath. The negligible thermal process of isomerization induced by the external heat-bath of fluid microenvironment as mentioned above (Fig. 7) indicates that the photo-isomerization in other microenvironments than in ethanol should have similar reactivity with it in ethanol, if the excess energy dissipation has the similar situation with it in fluid ethanol. The actual reactivities in the hybrid nano-layered environments, however, are very much different and remarkably enhanced ($\Phi_{cis–trans}$ = 1.9) (Table 2). These results strongly suggest that the situation of the energy dissipation is much different in the hybrid environment than that in ethanol.

In ethanol, the excess energy in the form of vibrational energy of C3F-Azo-C6H can be easily transferred to the surrounding solvent molecules and dissipates very efficiently through the microenvironment. However, in the solid state such as the hybrid nano-layered microenvironment, the excess energy may be difficult to dissipate as compared with that in solution. The low efficiency of *trans–cis* isomerization in the hybrid film also implies that a local heating around the molecule caused by the retarded dissipation of excess energy preferentially populates the *trans*-form by a locally heated thermal process. Very interestingly, the enhancement of *cis–trans* isomerization was not observed in the corresponding hydrocarbon analogue, C3H-Azo-C6H–SSA film. The polyfluoroalkyl chain thus should play a key role in the mechanism. The weak intermolecular interaction of the polyfluoroalkyl chain and the well-aligned bilayer structure within the interlayer spaces may cause the retardation of the heat energy dissipation to the surrounding environment. In this viewpoint, the order of the enhancement between the hybrid dry film ($\Phi_{cis–trans}$ = 1.9) > the film moistened with *n*-hexane ($\Phi_{cis\ to\ trans}$ = 1.1) > moistened with benzene ($\Phi_{cis–trans}$ = 0.94) ≫ in ethanol ($\Phi_{cis–trans}$ = 0.64) well rationalize the presumption. The hybrid film moistened with benzene exhibits an expansion of the interlayer distance to allow a penetration of benzene molecule into the interlayer, while *n*-hexane does not penetrate into the interlayer as demonstrated in Fig. S1 (ESI†). The intercalated benzene molecules would partly accept the excess energy like solvent molecules. From the viewpoint of the morphology change of the layered hybrids, such specific bilayer nanostructure, which could induce the local heating, may serve as a microenvironment to induce the large reversible morphology change. A laser flash photolysis study and microscopic temperature sensing experiments are now in progress to get direct evidence of the local heating in the nano-layered microenvironment.

Experimental

Materials

The polyfluorinated cationic azobenzene surfactant molecule (C3F-Azo-C6H) and corresponding hydrocarbon analogue (C3H-Azo-C6H), whose chemical structures are shown in Fig. 1b and c, were originally synthesized in our group.[2,3] Sumecton SA (SSA), which is a synthetic layered silicate with a saponite structure, was obtained from Kunimine Industries Co. Ltd and used as a host material without further purification. Benzene (spectroscopic grade, Kanto Chemical Co. Ltd), *n*-hexane (spectroscopic grade, Kanto Chemical Co. Ltd) and ethanol (99%, Shinwa Alcohol Industry Co., Ltd) were used as solvents for the swelling experiments. Ion-exchanged water (specific resistance $<0.1\ \mu S\ cm^{-1}$) was used for micelle formation.

Sample preparation and characterization

SSA (300 mg) was dispersed in 300 mL of ion-exchanged water and used as a stock dispersion for the preparation of hybrids. An aliquot of C3F-Azo-C6H aqueous solution for each loading level (1, 2, 3, 5, 7, 10, 15 eq.) *versus* cation exchange capacity (CEC) was added to 10 mL of SSA dispersion and stirred at 70 °C for 5 hours. The mixture was washed with ion-exchanged water and filtered by a hydrophilic polytetrafluoroethylene (PTFE) membrane (pore size of 0.1 μm, Advantec). After the filtration, the resulting hybrid was dried in vacuum and stored in the dark. The dried hybrids were analyzed by thermogravimetric/differential analysis (DTG-60H, Shimadzu), X-ray diffraction measurement (XRD, TINT-TTR III, Rigaku) and UV-vis absorption spectroscopy (UV-2550, Shimadzu). For the preparation of the hybrid film, the appropriate amount of hybrid dispersed in *n*-hexane was cast on the cover glass. The sample film was heated at 50 °C for 3 hours in the dark before the experiment to ensure that the azobenzene moiety was all in the *trans*-form. The sample film was also moistened with benzene or *n*-hexane for providing solvent-swelled microenvironment after inserting the film into the quartz cell (optical length: 1 cm).

Photoreaction of azobenzene

All the photo-irradiation experiments were carried out with a Xenon short arc lamp (500 W, USHIO) as the light source combining with an IR filter (IR cutoff filter, Edmond Optics) and band pass filters (MZ0365, ASAHI SPECTRA for 365 nm and MZ0440, ASAHI SPECTRA for 440 nm irradiation). UV (365 nm, 0.18 mW cm^{-2}) or visible light (440 nm, 6.5 mW cm^{-2}) irradiation of the sample solution or hybrid films was carried out for *trans–cis* and *cis–trans* isomerization reactions of azobenzene, respectively. The photoreactions were monitored by UV-vis spectroscopy.

 This journal is © the Owner Societies 2014

Published on 09 September 2014. Downloaded by Tokyo Metropolitan University on 23/10/2014 09:00:16.

The quantum yield of the photo-isomerization reaction was determined by the Fisher method from the initial slope of the number of molecules converted *versus* the number of photons adsorbed under two assumptions: (1) thermal isomerization is ignored and (2) quantum yield is constant at all wavelengths.[45] In addition, the internal filtering effect was taken into account for the calculation of the quantum yield for the *cis* to *trans* isomerization reaction because the masking effect due to a mixture of both *trans* and *cis* isomers should be removed for the calculation of quantum yield. In the photoreaction of the film, the scattering contribution of the sample was subtracted with the same amount of SSA film without C3F-Azo-C6H or C3H-Azo-C6H as a baseline.

Conclusions

We have systematically investigated the photoreactivity of the cationic polyfluoroalkyl azobenzene derivative C3F-Azo-C6H in different microenvironments. Compared with the photo-isomerization in ethanol, the quantum yield for the *trans* to *cis* photo-isomerization reaction of C3F-Azo-C6H was smaller in the clay-hybrid with SSA. On the other hand, the *cis–trans* isomerization reaction was remarkably enhanced and the quantum yield exceeded unity. The enhancement was partly explained by a possible change of level-crossing and energy state diagram which was evidenced by the changes of the activation energy for the conversion from *cis*- to *trans*-form in the more rigid microenvironment. The irregular enhancement of the quantum yield was only explainable by a cooperative effect among the azobenzene moieties packed in the bilayer structure of polyfluoroalkylated surfactants sandwiched by clay nanosheets. A presumption was postulated that a local heating around the molecule is induced by a retardation of dissipation of excess energy liberated through relaxation processes from the excited states as well as on the isomerization reaction pathway and the *trans*-form was preferentially populated at the locally elevated temperature. The well-aligned polyfluoroalkylated surfactants may provide the microenvironment for the retarded dissipation of the excess energy.

Acknowledgements

This work was partially supported by a Grant-in-Aid for Young Scientists (B) from the Ministry of Education, Culture, Sports, Science and Technology of Japan.

Notes and references

1 J.-M. Lehn, *Supramolecular Chemistry*, VCH, Weinheim, 1995.
2 Y. Nabetani, H. Takamura, Y. Hayasaka, S. Sasamoto, Y. Tanamura, T. Shimada, D. Masui, S. Takagi, H. Tachibana, Z. Tong and H. Inoue, *Nanoscale*, 2013, **5**, 3182–3193.
3 Y. Nabetani, H. Takamura, Y. Hayasaka, T. Shimada, S. Takagi, H. Tachibana, D. Masui, Z. Tong and H. Inoue, *J. Am. Chem. Soc.*, 2011, **133**, 17130–17133.
4 K. Nassau, J. W. Shiever and J. L. Bernstein, *J. Electrochem. Soc.*, 1969, **116**, 348–353.
5 A. D. Handoko and G. K. L. Goh, *Green Chem.*, 2010, **12**, 680–687.
6 X. Han, Q. Kuang, M. Jin, Z. Xie and L. Zheng, *J. Am. Chem. Soc.*, 2009, **131**, 3152–3153.
7 T. Sasaki and M. Watanabe, *J. Am. Chem. Soc.*, 1998, **120**, 4682–4689.
8 G. B. Saupe, C. C. Waraksa, H.-N. Kim, Y. J. Han, D. M. Kaschak, D. M. Skinner and T. E. Mallouk, *Chem. Mater.*, 2000, **12**, 1556–1562.
9 R. E. Schaak and T. E. Mallouk, *Chem. Mater.*, 2000, **12**, 3427–3434.
10 N. Miyamoto, K. Kuroda and M. Ogawa, *J. Mater. Chem.*, 2004, **14**, 165–170.
11 F. Geng, R. Ma, Y. Ebina, Y. Yamauchi, N. Miyamoto and T. Sasaki, *J. Am. Chem. Soc.*, 2014, **136**, 5491–5500.
12 J. N. Coleman, M. Lotya, A. O'Neill, S. D. Bergin, P. J. King, U. Khan, K. Young, A. Gaucher, S. De, R. J. Smith, I. V. Shvets, S. K. Arora, G. Stanton, H.-Y. Kim, K. Lee, G. T. Kim, G. S. Duesberg, T. Hallam, J. J. Boland, J. J. Wang, J. F. Donegan, J. C. Grunlan, G. Moriarty, A. Shmeliov, R. J. Nicholls, J. M. Perkins, E. M. Grieveson, K. Theuwissen, D. W. McComb, P. D. Nellist and V. Nicolosi, *Science*, 2011, **331**, 568–571.
13 T. Nakato, K. Kuroda and C. Kato, *Chem. Mater.*, 1992, **4**, 128–132.
14 M. Ogawa and K. Kuroda, *Chem. Rev.*, 1995, **95**, 399–438.
15 N. Sakai, Y. Ebina, K. Takada and T. Sasaki, *J. Am. Chem. Soc.*, 2004, **126**, 5851–5858.
16 T. Sasaki and M. Watanabe, *J. Phys. Chem. B*, 1997, **101**, 10159–10161.
17 G. Centi and S. Perathoner, *Microporous Mesoporous Mater.*, 2008, **107**, 3–15.
18 J. Yu, L. Qi and M. Jaroniec, *J. Phys. Chem. C*, 2010, **114**, 13118–13125.
19 Y. Miseki, H. Kato and A. Kudo, *Energy Environ. Sci.*, 2009, **2**, 306–314.
20 A. Kudo and Y. Miseki, *Chem. Soc. Rev.*, 2009, **38**, 253–278.
21 T. Tsukamoto, T. Shimada and S. Takagi, *J. Phys. Chem. A*, 2013, **117**, 7823–7832.
22 Y. Ishida, T. Shimada, H. Tachibana, H. Inoue and S. Takagi, *J. Phys. Chem. A*, 2012, **116**, 12065–12072.
23 Y. Ishida, T. Shimada, D. Masui, H. Tachibana, H. Inoue and S. Takagi, *J. Am. Chem. Soc.*, 2011, **133**, 14280–14286.
24 T. Yui, Y. Kobayashi, Y. Yamada, T. Tsuchino, K. Yano, T. Kajino, Y. Fukushima, T. Torimoto, H. Inoue and K. Takagi, *Phys. Chem. Chem. Phys.*, 2006, **8**, 4585–4590.
25 K. Maeda, M. Eguchi, S.-H. A. Lee, W. J. Youngblood, H. Hata and T. E. Mallouk, *J. Phys. Chem. C*, 2009, **113**, 7962–7969.
26 W. J. Youngblood, S.-H. A. Lee, K. Maeda and T. E. Mallouk, *Acc. Chem. Res.*, 2009, **42**, 1966–1973.

Published on 09 September 2014. Downloaded by Tokyo Metropolitan University on 23/10/2014 09:00:16.

27 P. Sun, X. Zhang, X. Liu, L. Wang, C. Wang, J. Yang and Y. Liu, *J. Mater. Chem.*, 2012, **22**, 6389–6393.
28 K. Maeda, M. Eguchi, W. J. Youngblood and T. E. Mallouk, *Chem. Mater.*, 2008, **20**, 6770–6778.
29 Y. Kameo, S. Takahashi, M. Krieg-Kowald, T. Ohmachi, S. Takagi and H. Inoue, *J. Phys. Chem. B*, 1999, **103**, 9562–9568.
30 H. Kusaka, M. Uno, M. Krieg-Kowald, T. Ohmachi, S. Kidokoro, T. Yui, S. Takagi and H. Inoue, *Phys. Chem. Chem. Phys.*, 1999, **1**, 3135–3140.
31 T. Yui, H. Yoshida, H. Tachibana, D. A. Tryk and H. Inoue, *Langmuir*, 2002, **18**, 891–896.
32 T. Yui, S. R. Uppili, T. Shimada, D. A. Tryk, H. Yoshida and H. Inoue, *Langmuir*, 2002, **18**, 4232–4239.
33 T. Yui, S. Fujii, K. Matsubara, R. Sasai, H. Tachibana, H. Yoshida, K. Takagi and H. Inoue, *Langmuir*, 2013, **29**, 10705–10712.
34 Z. Tong, S. Takagi, T. Shimada, H. Tachibana and H. Inoue, *J. Am. Chem. Soc.*, 2006, **128**, 684–685.
35 H. M. D. Bandara and S. C. Burdette, *Chem. Soc. Rev.*, 2012, **41**, 1809–1825.
36 N. Tamai and H. Miyasaka, *Chem. Rev.*, 2000, **100**, 1875–1890.
37 T. Fujino, S. Y. Arzhantsev and T. Tahara, *Bull. Chem. Soc. Jpn.*, 2002, **75**, 1031–1040.
38 T. Fujino and T. Tahara, *J. Phys. Chem. A*, 2000, **104**, 4203–4210.
39 S. Takagi, M. Eguchi, D. A. Tryk and H. Inoue, *J. Photochem. Photobiol., C*, 2006, **7**, 104–126.
40 M. Kasha, H. R. Rawls and M. Ashraf El-Bayoumi, *Pure Appl. Chem.*, 1965, **11**, 371.
41 I. K. Lednev, T.-Q. Ye, L. C. Abbott, R. E. Hester and J. N. Moore, *J. Phys. Chem. A*, 1998, **102**, 9161–9166.
42 T. Schultz, J. Quenneville, B. Levine, A. Toniolo, T. J. Martínez, S. Lochbrunner, M. Schmitt, J. P. Shaffer, M. Z. Zgierski and A. Stolow, *J. Am. Chem. Soc.*, 2003, **125**, 8098–8099.
43 J. B. Birks, *Photophysics of Aromatic Molecules*, John Wiley & Sons, Ltd, New york, 1970, pp. 110–112.
44 N. J. Turro, V. Ramamurthy and J. C. Scaiano, *Principles of Molecular Photochemistry An Introduction*, University Science Book, California, 2009, pp. 265–317.
45 E. Fischer, *J. Phys. Chem.*, 1967, **71**, 3704–3706.

 This journal is © the Owner Societies 2014